# Noncontact Manipulation of Magnetic Objects with an Array of Permanent Magnets and Linear Servomotors

Lahiru Ekanayake, Janaka Madhusanka, and Arash Komaee

Abstract—This paper presents the concept, implementation, feedback control, and experimental verification of a noncontact magnetic manipulator that relies on a controllable array of permanent magnets to manipulate magnetized objects inside a workspace encircled by the magnets. To gain control over the aggregate magnetic field inside the workspace, the position of each magnet is independently controlled by a linear servomotor that dynamically changes the distance between that magnet and the workspace. By feedback control of the array of servomotors, the magnetic force applied to a magnetized object inside the workspace is dynamically adjusted to steer it along a desired reference trajectory. The successful steering of a small magnetic bead is demonstrated by experiments performed on a planar magnetic manipulator, designed and prototyped with six linear servomotors and six permanent magnets.

### I. INTRODUCTION

This paper presents preliminary results from our ongoing work on noncontact magnetic manipulation based on arrays of permanent magnets and linear servomotors (LSM). The magnetic manipulator proposed in this paper is schematically illustrated in Fig. 1 and consists of an array of six axially magnetized permanent magnets, each independently actuated by an LSM to effectively control its distance from a circular workspace. The aggregate magnetic field generated by the array of magnets and controlled by the array of servomotors is then leveraged to exert force on magnetized objects inside the workspace, aimed to drive them in desired directions. By feedback control of the array of servomotors, the magnetized objects can be effectively steered along reference trajectories within the workspace.

The magnetized object controlled inside the workspace can be, for instance, a magnetically tipped catheter or any other medical devices used for non- or minimally invasive surgical, imaging, or drug delivery procedures [1]–[11]. These devices can be safely navigated inside the patients' natural pathways by means of external magnetic fields produced and controlled by a magnetic manipulator such as the one introduced in this paper. For medical applications, magnetic manipulators often need to produce relatively strong magnetic fields at distances as far as several decimeters, which are more technically feasible and economically viable to produce using permanent magnets rather than electromagnets with substantially larger size, weight, and cost [12]. Hence, the magnetic manipulator proposed in this paper offers a more compact, less expensive alternative to the existing electromagnet-based designs.

This work was supported by the National Science Foundation under Grant No. ECCS-1941944.

The authors are with the School of Electrical, Computer, and Biomedical Engineering, Southern Illinois University, Carbondale, IL, 62901 USA email: {lahiru.ekanayake, janakamwm, akomaee}@siu.edu.

The magnetic manipulator in this paper is composed of six magnetomechanical units shown in Fig. 2, each consisting of a permanent magnet bar and a linear actuator to adjust its position along a nonmagnetic guiding cylinder. Each of the units effectively emulates an electromagnet, and can replace electromagnets in well established existing designs such as OctoMag [13]. An important advantage of the proposed units is that by pulling their magnets back from the workspace, their magnetic fields can be practically turned off, as a safety requirement not provided by other permanent magnet-based designs [14]–[17].

To realize and experimentally validate the early concept of this paper, we developed a benchtop experimental setup and an early-stage feedback law for its closed-loop control. This feedback law is aimed to drive a magnetic bead along desired reference trajectories in the workspace of the experimental setup by measuring its real-time position and correcting its trajectory accordingly via the LSMs that control the magnetic field inside the workspace. The control design procedure in this paper is mainly inspired by our earlier work on magnetic manipulators with rotatable permanent magnets [17].

The rest of this paper is organized as follows. In Section II, first the concept of magnetic manipulation using permanent magnets and linear actuators is presented, and then, the implementation of this concept as an experimental setup is discussed. Next in Section III, the dynamics of this set up is modeled by a set of nonlinear state-space equations, which is exploited in Section IV to develop a feedback control law. Finally, experimental and simulation results are presented in Section V to evaluate the performance of the developed setup under feedback control.

## II. BASIC CONCEPT AND SYSTEM DESIGN

The magnetic manipulator proposed in this paper relies on arrays of magnetomechanical units encircling a workspace in which magnetic objects can be manipulated without direct contact. Each of these units consists of an axially magnetized permanent magnet attached to a servomotor that can move it back and forth inside a nonmagnetic guiding cylinder. Fig. 2 shows a prototype of such units developed in this work, and Fig. 1 schematically illustrates a planar magnetic manipulator formed by placing six of these units at equal distances around a circular workspace. Obviously, 3D magnetic manipulators can be developed based on 3D arrangements of a suitable number of these magnetomechanical units.

The total magnetic field produced by the magnets of these units can be effectively controlled inside the workspace via controlling the distances of the magnets from the workspace

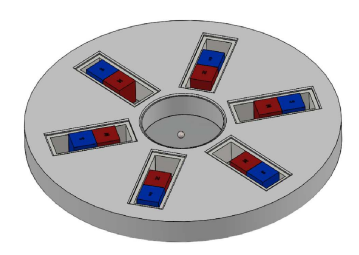


Fig. 1. Schematic diagram of the magnetic manipulator proposed in this paper with 6 axially magnetized permanent magnets around a circular workspace. The magnetic field inside this workspace is controlled by 6 servomotors via adjusting the distances of the magnets from the workspace.



Fig. 2. Prototyped magnetomechanical unit consists of a permanent magnet (inside the green holder) moving back and forth inside a nonmagnetic guiding cylinder (white) using an LSM (black).

using the servomotors embedded in the units. This magnetic field interacts with magnetic objects inside the workspace to exert a controllable magnetic force on them, through which, they can be driven in desired directions. By feedback control of the magnetic force, the magnetic objects are then steered along desired reference trajectories inside the workspace. The feedback loop is established by measuring the positions of these objects in real time, and feeding the measured values to control algorithms that provide inputs to the servomotors.

To experimentally prove the proposed concept of magnetic manipulation, we developed the benchtop experimental setup of Fig. 3 to realize the magnetic manipulator of Fig. 1. This setup utilizes six magnetomechanical units in Fig. 2, and a high-speed camera fixed above the workspace to measure the real-time position of a magnetic bead steered along reference trajectories inside the workspace. This magnetic bead resides inside a Petri dish housed within the workspace and filled with a viscous fluid (corn syrup). For feedback control of the magnetic bead, we developed an early-stage control law (12), which was implemented on a desktop computer running the real-time software LabVIEW. In addition, built-in modules of LabVIEW were utilized to extract the position of magnetic bead from the images captured by the camera in real time.

## A. Experimental Setup

The experimental setup of Fig. 3 consists of several parts and components, each separately designed using SolidWorks and fabricated by 3D printing. The individual components were next installed on a 3D-printed foundation that provides six slots for installation of six magnetomechanical units in Fig. 2, a holder for the Petri dish housing the magnetic bead, and three holders for an adjustable camera mount. A 3-screw mechanism was embedded in the foundation for its horizontal adjustment using two orthogonal spirit levels. The structure

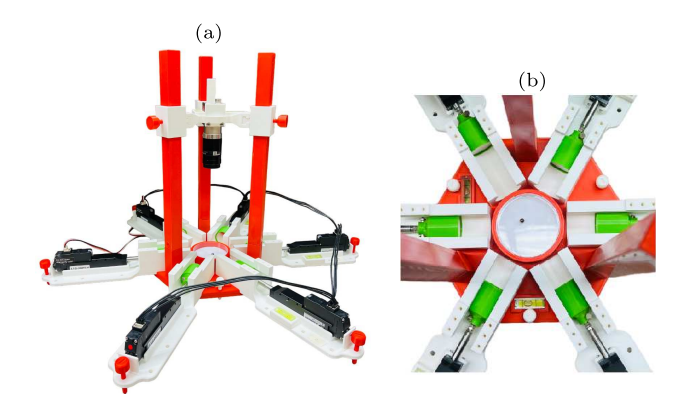


Fig. 3. Prototyped magnetic manipulator with 6 permanent magnet bars evenly spaced around a circular workspace containing a magnetic bead. A high-speed camera positioned on top of the workspace is utilized to estimate the position of the magnetic bead to establish a feedback loop.

and design of the components comprising the setup of Fig. 3 are discussed below.

- 1) Magnetomechanical Unit: The main component of the setup of Fig. 3 is the magnetomechanical unit of Fig. 2. This unit consists of a cylindrical magnet bar attached to the rod end of an LSM, both housed in a 3D-printed rigid structure. The magnet bar is a grade N52, NdFeB, axially magnetized cylinder of diameter 25.4 mm and height 25.4 mm, with a strong surface field of 662 mT. The LSM is a mightyZAP model L12-20PT-6 with 34 N maximum load, 80 mm/sec maximum speed, and 56 mm stroke. It is attached to the magnet by a 3D-printed connector that houses the magnet in one side and connects to the rod end of the LSM from the other side.
- 2) Workspace and Magnetic Object: The workspace is a flat, circular area of diameter 64 mm, which can hold Petri dishes of different diameters up to 64 mm. For experiments in this work, a Petri dish of diameter 39 mm was used, and was filled with transparent corn syrup to allow for optical tracking of a magnetic bead inside the Petri dish. This magnetic bead was chosen as a sphere of 3 mm diameter and 0.11 gm mass, made of steel with a magnetic susceptibility of 1000.
- 3) Camera and Its Adjustable Mount: For tracking the magnetic bead inside the workspace, the developed setup was equipped with an Allied Vision Alvium 1800 U-158 camera with a Moritex 5 Mpixel lens. This camera has a maximum frame rate of 257 fps at 1.6 Mpixel. The video feed from this camera is processed in real time by the Vision Assistant module of LabVIEW relying on a computer vision algorithm to estimate the position of the magnetic bead.

To properly focus the camera on the workspace, it is installed on a 3D-printed adjustable mount, which is rigidly attached to the foundation of the developed setup. The camera mount can adjust the distance of the camera from the workspace to attain the widest field of view and the highest image resolution, which in turn, leads to the most accurate estimates for the position of the magnetic bead. A pair of orthogonal spirit levels are embedded in the camera mount to adjust the axis of camera perpendicular to the workspace.

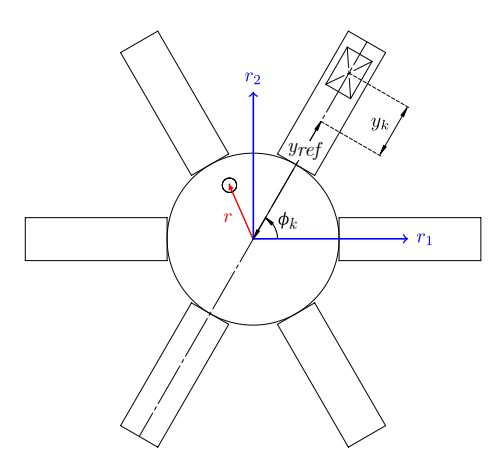


Fig. 4. Planar diagram of the magnetic manipulator of Fig. 3 illustrating a coordinate system ( $r_1$  and  $r_2$  denote its two orthogonal axes) fixed at the center of workspace, the position vector r of the magnetic bead in that coordinate system, and a reference point for the position of magnet k.

## III. SYSTEM DYNAMICS

This section follows [15]–[17] to develop a set of nonlinear state-space equations that represent the motion of a magnetic bead moving in a viscous fluid inside the workspace of the magnetic manipulator of Fig. 1. The magnetic bead has a mass m and moves under the total magnetic force  $f_{mag}\left(r,y\right)$  generated by all magnets, and the Stokes' drag  $f_{drag}\left(v\right)$  (fluid friction) according to Newton's second law of motion

$$m\dot{v}(t) = f_{mag}(r(t), y(t)) + f_{drag}(v(t)). \tag{1}$$

Here,  $r\left(t\right)$  is a 2-dimensional vector representing the planar position of the magnetic bead at time t with respect to the coordinate system of Fig. 4, and  $v\left(t\right)=\dot{r}\left(t\right)$  is its velocity in the same coordinate system. The magnetic force  $f_{mag}\left(r,y\right)$  is a function of the position r of the magnetic bead, and also, the positions of all 6 permanent magnets, gathered into the 6-dimensional vector y. The Stokes' drag  $f_{drag}\left(v\right)$  is known to be proportional to the velocity v of the magnetic bead [18], i.e.,  $f_{drag}\left(v\right)=-\mu v$ , where  $\mu$  is a positive constant that depends on the size of the magnetic bead and the viscosity of its surrounding fluid.

By defining the constant  $\sigma = \mu/m$  and the vector function

$$g(r,y) = \frac{f_{mag}(r,y)}{m},$$
(2)

the Newton's second law (1) is rewritten as

$$\dot{v}(t) = -\sigma v(t) + g(r(t), y(t)). \tag{3}$$

The vector function g(r,y) in (2) represents magnetic force per unit of mass or magnetic acceleration, and is determined in Section III-A for the magnetic manipulator of Fig. 1.

The vector y in (2) contains the elements  $y_1, y_2, \ldots, y_6$ , each representing the position of a permanent magnet with respect to the center of workspace, as shown in Fig. 4. In particular,  $y_k$  denotes the position of the center of magnet  $k=1,2,\ldots,6$  along the direction

$$\rho_k = \begin{bmatrix} \cos \phi_k \\ \sin \phi_k \end{bmatrix}, \quad \phi_k = \frac{(k-1)\pi}{3}, \tag{4}$$

and with respect to a point at a distance  $y_{ref}$  from the center of workspace.

The control input to the magnetic manipulator of Fig. 1 is a 6-dimensional vector u(t) containing the reference signals  $u_1(t), u_2(t), \ldots, u_6(t)$  to 6 servomotors, each controlling the position  $y_k(t)$  of its corresponding permanent magnet. The relationship between the output  $y_k(t)$  and input  $u_k(t)$  of each servomotor is described by a second-order linear dynamics [19] via the transfer function

$$H_{\text{servo}}(s) = \frac{\omega_n^2}{s^2 + 2\zeta\omega_n s + \omega_n^2},$$

where  $\omega_n$  and  $\zeta$  are positive constants known as the natural frequency and damping ratio of the servomotor, respectively.

By representing this transfer function in time domain and in vector form, and then concatenating the resulting equations with  $\dot{r}(t) = v(t)$  and Newton's second law (3), the dynamics of the magnetic manipulator is expressed by the nonlinear state-space equations

$$\dot{r}\left(t\right) = v\left(t\right) \tag{5a}$$

$$\dot{v}(t) = -\sigma v(t) + g(r(t), y(t)) \tag{5b}$$

$$\dot{y}\left(t\right) = v_{y}\left(t\right) \tag{5c}$$

$$\dot{v}_y(t) = -\omega_n^2 y(t) - 2\zeta \omega_n v_y(t) + \omega_n^2 u(t). \tag{5d}$$

Here,  $v_y(t)$  is a vector containing 6 servomotor velocities.

# A. Modeling of Magnetic Acceleration

The magnetic field at a point r inside the workspace of the magnetic manipulator of Fig. 1 is generated by 6 magnets located at points represented by the vector y. This magnetic field, denoted by  $h\left(r,y\right)$ , is the source of the magnetic force  $f_{mag}\left(r,y\right)$  inside the workspace. The relationship between these two fields is known [20] to be

$$f_{mag}(r,y) = k_m \nabla \|h(r,y)\|^2,$$
 (6)

where  $k_m$  is a positive constant depending on the volume and permeability of the magnetic object receiving the force,  $\nabla$  is the operator of gradient with respect to r, and  $\|\cdot\|$  denotes the Euclidean norm of vectors. By defining  $H(\cdot)$  as the  $2\times 2$  Jacobian matrix of  $h(\cdot)$  with respect to r and dividing both sides of (6) by m, the magnetic acceleration is obtained as

$$g(r,y) = \frac{2k_m}{m} H(r,y) h(r,y).$$
 (7)

A mathematical model of  $h\left(r,y\right)$  is developed in the rest of this section.

Consider a coordinate system attached to magnet k with its first axis aligned with  $-\rho_k$  defined in (4), and its other axis perpendicular to  $\rho_k$ . In this coordinate system, the magnetic field of this magnet is denoted by  $h_c\left(r'\right)$ . Referring to Fig. 4, let r be a point in the circular workspace, represented in the  $r_1-r_2$  coordinate system at the center of the workspace. This same point is represented in the coordinate system attached to the magnet k as

$$r_k' = R_k^T \left( r - \left( y_{ref} + y_k \right) \rho_k \right),\,$$

where  $R_k$  is a rotation matrix given by

$$R_k = -\begin{bmatrix} \cos \phi_k & -\sin \phi_k \\ \sin \phi_k & \cos \phi_k \end{bmatrix}.$$

The total magnetic field h(r, y) is the superposition of 6 individual magnetic fields, with the contribution of magnet k given by  $R_k h_c(r'_k)$ , that is

$$h(r,y) = \sum_{k=1}^{6} R_k h_c \left( R_k^T \left( r - \left( y_{ref} + y_k \right) \rho_k \right) \right).$$

The Jacobian matrix of this vector field is readily obtained as

$$H(r,y) = \sum_{k=1}^{6} R_k H_c \left( R_k^T (r - (y_{ref} + y_k) \rho_k) \right) R_k^T$$

in terms of the Jacobian matrix  $H_c\left(\cdot\right)$  of  $h_c\left(\cdot\right)$ . Throughout this paper,  $h_c\left(\cdot\right)$  and its partial derivatives are computed numerically via a combination of COMSOL finite element simulations and least squares interpolation techniques.

### IV. CONTROLLER DESIGN

For early experiments on the experimental setup of Fig. 3, a simple linear controller is designed as a point of departure. We are currently working to develop more effective control laws based on more advanced control techniques such as feedback linearization [16]. Our current linear controller is designed based on an approximate model derived from the nonlinear state-space equation (5) by linearizing it around its equilibrium point at  $(r, v, y, v_y) = (0, 0, 0, 0)$ .

Based on the geometric symmetry of the magnets around the center of workspace, it can be verified that  $g\left(0,0\right)=0$ . Then, the magnetic acceleration  $g\left(r,y\right)$  can be approximated by the first two terms of its Taylor series as

$$g(r,y) \simeq G_r(0,0) r + G_y(0,0) y,$$
 (8)

where  $G_r\left(\cdot\right)$  and  $G_y\left(\cdot\right)$  denote the  $2\times 2$  and  $2\times 6$  Jacobian matrices of  $g\left(\cdot\right)$  with respect to r and y, respectively. Again, as a result of geometric symmetry,  $G_r\left(0,0\right)$  is diagonal with equal diagonal elements  $\alpha$ , i.e.,  $G_r\left(0,0\right)=\alpha I_{2\times 2}$ , where  $I_{2\times 2}$  denotes the  $2\times 2$  identity matrix. Also, the Jacobian matrix  $G_y\left(\cdot\right)$  is denoted by B, for the sake of simplicity. Then, by replacing (8) into (5b), the nonlinear dynamics of the magnetic manipulator is approximated by the linear statespace equations

$$\dot{r}\left(t\right) = v\left(t\right) \tag{9a}$$

$$\dot{v}(t) = \alpha r(t) - \sigma v(t) + B y(t) \tag{9b}$$

$$\dot{y}\left(t\right) = v_{y}\left(t\right) \tag{9c}$$

$$\dot{v}_{y}\left(t\right) = -\omega_{n}^{2} y\left(t\right) - 2\zeta\omega_{n} v_{y}\left(t\right) + \omega_{n}^{2} u\left(t\right). \tag{9d}$$

The control mission is to drive a small magnetic bead along planar reference trajectories near the center of circular workspace in the magnetic manipulator of Fig. 3. This goal requires our designed controller to maintain the position  $r\left(t\right)$  of the magnetic bead close to a reference trajectory  $r_{d}\left(t\right)$ . To control the 2-dimensional output vector  $r\left(t\right)$ , only 2 degrees of freedom out of 6 control variables of  $u\left(t\right)$  are required.

Therefore, the control  $u\left(t\right)$  can be constrained to stay in the column space of  $B^{T}$  by defining the 2-dimensional auxiliary control  $z\left(t\right)$  and generating  $u\left(t\right)$  according to

$$u\left(t\right) = B^{T} \left(BB^{T}\right)^{-1} z\left(t\right).$$

Substituting this expression into (9d) and then applying Laplace transform to the linear state-space equations (9), the relationship between  $r\left(t\right)$  and  $z\left(t\right)$  can be expressed in the Laplace domain as

$$R(s) = H(s) Z(s), \qquad (10)$$

where R(s) and Z(s) are 2-dimensional vectors denoting the Laplace transforms of r(t) and z(t), respectively, and the transfer function H(s) is given by

$$H(s) = \frac{1}{s^2 + \sigma s - \alpha} \cdot \frac{\omega_n^2}{s^2 + 2\zeta\omega_n s + \omega_n^2}.$$
 (11)

It is observed from (10) that the dynamics of the first and the second elements of  $r\left(t\right)$  are decoupled and are controlled independently by the first and the second elements of  $z\left(t\right)$  via the transfer function (11). For each of these single-input-single-output dynamics, a proportional controller is designed by the root locus of the transfer function (11). With a gain  $k_p$ , the resulting controller is expressed in the vector form

$$u(t) = -k_p B^T (BB^T)^{-1} (r(t) - r_d(t)).$$
 (12)

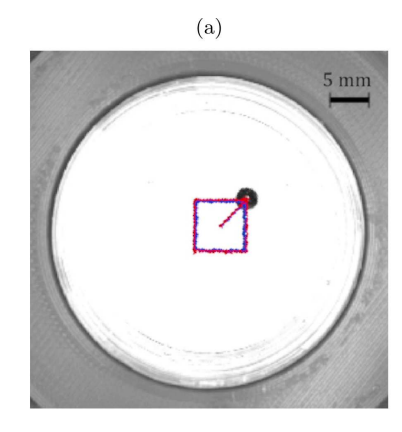
The performance of this feedback law is evaluated next by experiments.

## V. EXPERIMENTAL RESULTS

The feedback control (12) was implemented as a module in the graphical environment of LabVIEW, updating the control value every 96 msec. A gain value of  $k_p=121$  was initially obtained for this control using the root locus method with the parameter values  $\omega_n=39.8$  rad/sec,  $\zeta=0.7, \sigma=415$  1/sec, and  $\alpha=72.3$  1/sec<sup>2</sup> for the transfer function (11). Then, by observing the performance of the controller in practice, the numerical value of gain was fine-tuned to  $k_p=66$  for the best performance. This value was used for experiments under different reference trajectories shown in Figs. 5, 8, and 9.

In the experiments, the reference input  $r_d\left(t\right)$  was changed in small steps, with a maximum deviation of 0.5 mm in each direction. Also, the time interval between each incremental change was maintained at a minimum of 1 sec, allowing the magnetic bead to reach the steady-state in each small step. The experimental results were compared with their simulated counterparts in order to investigate possible discrepancies between the experimental setup and its mathematical model.

In the first experiment, a square of 6 mm side length centered at the origin was adopted as the reference trajectory, shown in blue in Fig. 5. At the beginning of the experiment t=0, the magnetic bead was positioned at the origin, and then, the reference input  $r_d(t)$  was changed from (0,0) mm to (3,3) mm in small steps. This segment of the reference trajectory is shown (in blue) more clearly in Fig. 6(a). Next,



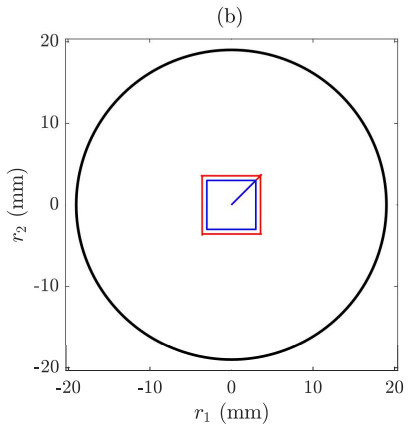
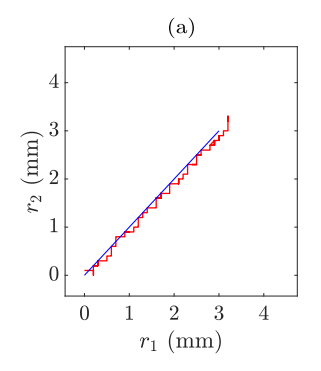


Fig. 5. Trajectory of a magnetic bead (red) tracking a square-shaped reference (blue) of side length 6 mm, generated by (a) experiment, and (b) computer simulation.

starting from (3,3) mm, the reference input was changed until completing the trajectory. The trajectory of the magnetic bead is shown (in red) in Figs. 5(a) and 6(a).

It is observed from these figures that the magnetic bead closely tracks the reference trajectory, while the simulation results in Figs. 5(b) and 6(b) indicate a significant deviation from this trajectory. This observation can be explained by a mismatch between the experimental setting and the model parameters. The first element  $r_1\left(t\right)$  of the position  $r\left(t\right)$  is illustrated versus time in Fig. 7 for the same experiment of Fig. 6. Even though the simulation results demonstrate a relatively large tracking error, this error is much smaller for experiment. Completing the entire reference trajectory has taken around 35 sec for the actual magnetic manipulator, versus 30 sec for its simulator.

Next, the control performance was evaluated when  $r_d\left(t\right)$  changes at large steps. For this purpose, a square of 4 mm side length was considered, and the reference input  $r_d\left(t\right)$  was abruptly changed from one vertex to another within 1 sec for each jump, starting from the first vertex (2,2) mm. The trajectory of the magnetic bead under this reference input is shown in Fig. 8. Instead of travelling 3 mm within 35 sec in Fig. 7, the magnetic bead in Fig. 8 travels 16 mm in 4 sec at a much higher speed. However, closely observing the path traced by the magnetic bead in Fig. 8 indicates an increased



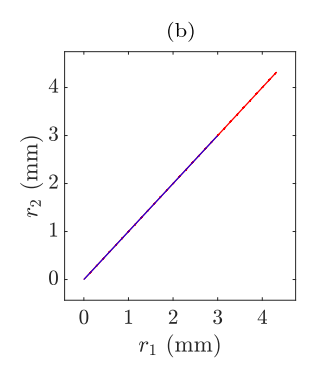


Fig. 6. Comparison of the trajectories of magnetic bead (red) generated by (a) experiment and (b) simulation for a reference input (blue) changing from (0,0) to (3,3).

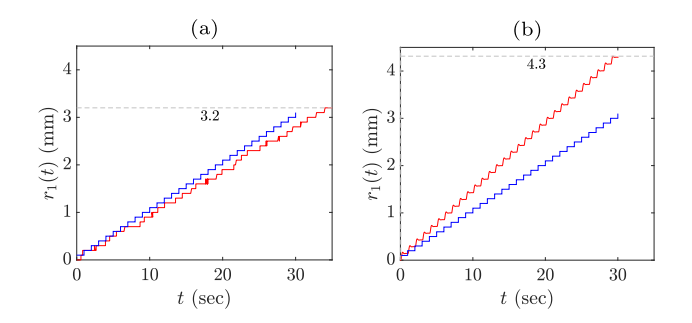


Fig. 7. Position of magnetic bead along  $r_1$  axis versus time (red), generated for the same reference trajectory (blue) of Fig. 6 by (a) experiment and (b) simulation.

tracking error compared to that of Fig. 5(a).

In the last experiment, the path tracking performance was evaluated for more complex reference trajectories in Fig. 9. A major observation in this experiment is a gradual increase in the tracking error as the magnetic bead moves away from the center of workspace. Since the controller was designed based on a linearized model, the most likely cause of this observation is the nonlinearity of the magnetic manipulator, not reflected in its approximate linear model, particularly as the magnetic bead moves away from the equilibrium point.

# VI. CONCLUSION

A novel concept for magnetic manipulation was proposed, implemented as a benchtop setup, and validated by a series of experiments. Magnetic manipulation by this concept relies on arrays of magnetomechanical units consisting of permanent magnets moving back and forth inside nonmagnetic guiding cylinders. Each of these units effectively emulates the same functions of an electromagnet in generation and control of magnetic fields, but control over the magnetic field is gained in these units by adjusting the position of magnets inside their guiding cylinders, versus terminal voltages in the case of electromagnets. At similar strength of magnetic field, these units can be manufactured smaller in size and weight and less expensive in cost, and therefore, offer a viable alternative to electromagnets, in particular for medical applications which often need strong magnetic fields at relatively far distances.

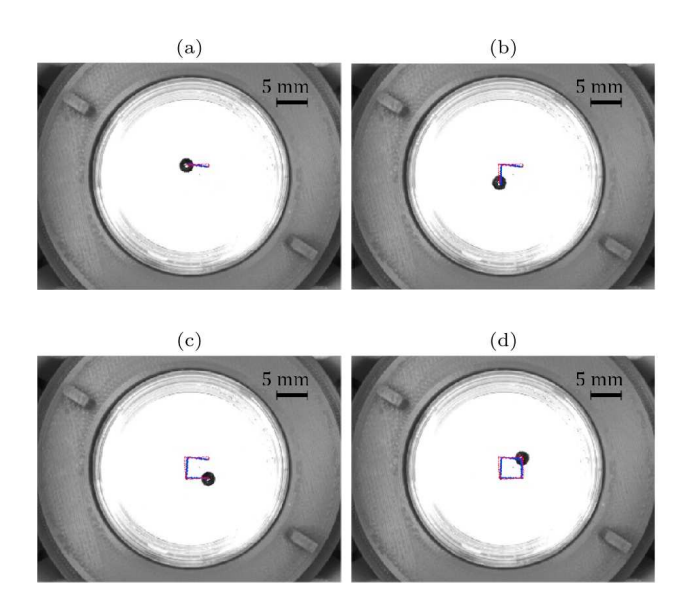


Fig. 8. Magnetic bead tracking (red) a square-shaped reference trajectory (blue) of 4 mm side length under the control law (12). Starting at t=0, Figs. 8(a) through 8(d) have been recorded at  $t=1.00\,$  sec,  $t=1.90\,$  sec,  $t=3.10\,$  sec, and  $t=4.10\,$  sec, respectively.

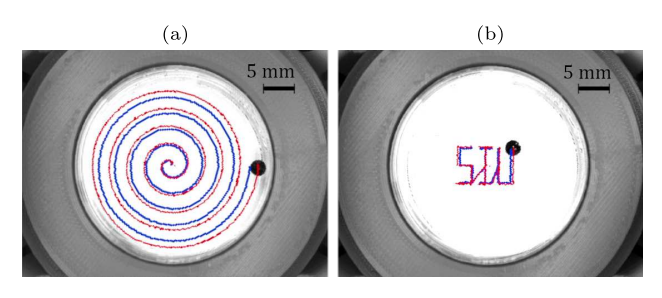


Fig. 9. Trajectories of a magnetic bead (red) tracking complex references (blue): (a) spiral trajectory with 15 mm maximum distance from the center; and (b) SIU-shaped trajectory. The tracking error grows considerably large with the distance from the center of workspace.

## REFERENCES

- V. Iacovacci, E. Diller, D. Ahmed, and A. Menciassi, "Medical microrobots," *Annual Review of Biomedical Engineering*, vol. 26, 2024.
- [2] W. G. Lee, L. L. Evans, and M. R. Harrison, "Beyond the gut: Spectrum of magnetic surgery devices," *Frontiers in Surgery*, vol. 10, p. 1253728, 2023.
- [3] Q. Fu, X. Zhang, S. Zhang, C. Fan, Z. Cai, and L. Wang, "A magnetically capsule robot for biomedical application," *Applied Bionics and Biomechanics*, vol. 2022, p. 2233417, 2022.
- [4] P. Blümler, "magnetic guiding with permanent magnets: Concept, realization and applications to nanoparticles and cells," *Cells*, vol. 10, no. 10, p. 2708, 2021.

- [5] D. Vlaskou, O. Mykhaylyk, and C. Plank, "Magnetic and acoustically active microbubbles loaded with nucleic acids for gene delivery," *Methods in Molecular Biology*, vol. 1943, pp. 253–290, 2019.
- [6] A. Z. Taddese, P. R. Slawinski, M. Pirotta, E. De Momi, K. L. Obstein, and P. Valdastri, "Enhanced real-time pose estimation for closed-loop robotic manipulation of magnetically actuated capsule endoscopes," *The International Journal of Robotics Research*, vol. 37, no. 8, pp. 890–911, 2018.
- [7] T. Cheng, C. S. H. Ng, P. W. Y. Chiu, and Z. Li, "Design and prototyping of a soft magnetic anchored and guidance endoscope system," in *Proc. of 2017 IEEE/RSJ International Conference on Intelligent Robots and Systems (IROS)*, pp. 2902–2908, 2017.
- [8] S. Yim and M. Sitti, "Design and rolling locomotion of a magnetically actuated soft capsule endoscope," *IEEE Transactions on Robotics*, vol. 28, no. 1, pp. 183–194, 2012.
- [9] S. Yim and M. Sitti, "Shape-programmable soft capsule robots for semi-implantable drug delivery," *IEEE Transactions on Robotics*, vol. 28, no. 5, pp. 1198–1202, 2012.
- [10] J. L. Toennies, G. Tortora, M. Simi, P. Valdastri, and R. J. Webster, "Swallowable medical devices for diagnosis and surgery: the state of the art," *Proc. of the Institution of Mechanical Engineers, Part C: Journal of Mechanical Engineering Science*, vol. 224, no. 7, pp. 1397– 1414, 2010.
- [11] G. Ciuti, P. Valdastri, A. Menciassi, and P. Dario, "Robotic magnetic steering and locomotion of capsule endoscope for diagnostic and surgical endoluminal procedures," *Robotica*, vol. 28, no. 2, pp. 199– 207, 2010.
- [12] O. Baun and P. Blümler, "Permanent magnet system to guide superparamagnetic particles," *Journal of Magnetism and Magnetic Materi*als, vol. 439, pp. 294–304, 2017.
- [13] M. P. Kummer, J. J. Abbott, B. E. Kratochvil, R. Borer, A. Sengul, and B. J. Nelson, "OctoMag: An electromagnetic system for 5-DOF wireless micromanipulation," *IEEE Transactions on Robotics*, vol. 26, no. 6, pp. 1006–1017, 2010.
- [14] P. Ryan and E. Diller, "Magnetic actuation for full dexterity microrobotic control using rotating permanent magnets," *IEEE Transactions* on *Robotics*, vol. 33, no. 6, pp. 1398–1409, 2017.
- [15] N. Riahi and A. Komaee, "Steering magnetic particles by feedback control of permanent magnet manipulators," in *Proc. of 2019 American Control Conference (ACC 2019)*, pp. 5432–5437, 2019.
- [16] N. Riahi, L. R. Tituaña, and A. Komaee, "Homotopy continuation for feedback linearization of noncontact magnetic manipulators," in *Proc.* of 2020 American Control Conference (ACC 2020), pp. 4295–4300, 2020.
- [17] N. Riahi and A. Komaee, "Noncontact steering of magnetic objects by optimal linear feedback control of permanent magnet manipulators," in *Proc. of 2020 IEEE/ASME International Conference on Advanced Intelligent Mechatronics (AIM 2020)*, pp. 30–35, 2020.
- [18] R. Probst, J. Lin, A. Komaee, A. Nacev, Z. Cummins, and B. Shapiro, "Planar steering of a single ferrofluid drop by optimal minimum power dynamic feedback control of four electromagnets at a distance," *Journal of Magnetism and Magnetic Materials*, vol. 323, no. 7, pp. 885–896, 2011.
- [19] M. Mohammadzadeh, M. R. Shariatmadari, N. Riahi, and A. Komaee, "Feedback decoupling of magnetically coupled actuators," in *Proc. of the 2021 IEEE/ASME International Conference on Advanced Intelligent Mechatronics (AIM 2021)*, pp. 320–325, 2021.
- [20] Q. A. Pankhurst, J. Connolly, S. K. Jones, and J. Dobson, "Applications of magnetic nanoparticles in biomedicine," *Journal of Physics* D: Applied Physics, vol. 36, no. 13, p. R167, 2003.